Metamaterial-Based Analog Recurrent Neural Network Toward Machine Intelligence

Tianxi Jiang[,1] Tianqi Li,[1] Hao Huang,[1] Zhi-Ke Peng,[1,2] and Qingbo He[1,*]

[1]*State Key Laboratory of Mechanical System and Vibration, Shanghai Jiao Tong University, 200240 Shanghai, People's Republic of China*

[2]*School of Mechanical Engineering, Ningxia University, 750021 Yinchuan, People's Republic of China*

Wave-based analog computation platforms hold the promise of realizing intelligent information processing with high speed and low computational cost, but current design principles face intractable problems in processing low-frequency wave information end to end at the physical layer. Here we theoretically demonstrate a concept of a metamaterial-based analog recurrent neural network (Meta-RNN) for intelligent classification of physical information carried by mechanical vibrations. With the spatiotemporal recurrence relation induced by coupled local resonators of the simulated metamaterial model, the Meta-RNN is capable of memorizing the internal hidden state in the dynamic displacement field. The trained coupling and synergy of local resonators lead to desirable vibration energy localization with selective frequency extraction capability, which can distinguish the intrinsic characteristics of vibration information. The proposed Meta-RNN provides a foundation for implementing a promising mechanical analog processor for intelligent vibration information processing and classification, and paves the way to efficient machine learning platforms for machine intelligence.

DOI: 10.1103/PhysRevApplied.19.064065

I. INTRODUCTION

Mechanical vibrations are ubiquitous in daily life, from human activity to the operation of mechanical systems. Discovering the physical information contained in vibration signals is essential not only in health monitoring and clinical diagnosis [1,2], but also in human-machine interaction and the Internet of things [3,4], such as virtual reality [5], home automation [6], and smart industrial infrastructure [7]. Specifically, vibration sensing can endow mechanical systems with the intelligence to perceive their own states and make corresponding decisions [8–10]. The most common framework for vibration sensing is organized in a sequential way. Sensor signals are amplified and filtered, and then converted to digital signals by using an analog-to-digital conversion (ADC) device. The information can be extracted by employing post-processing methods including statistical analysis, machine learning, and artificial intelligence.

Among these processing methods, the artificial neural network (ANN) is a powerful tool that can garner meaningful knowledge from sensor data and has achieved remarkable success over the past decade in performing complex intelligent information processing, such as computer vision, speech recognition, and natural language processing [11–13]. The superior performance of ANNs has revolutionized the design paradigm of materials [14], proteins [15], and metastructures [16–18]. Currently, ANNs are typically implemented using traditional von Neumann computing architectures. The requirement of ADC and data transfer between memory and logic devices consume significant time and power [19]. With the increase in modern devices and data, the computational demands of ANNs are dramatically increasing, prompting efforts to develop new hardware platforms with high speed and low power consumption [19–21], such as neuromorphic computing with memristors [22–24].

One attractive approach is to use artificially engineered structures, such as metasurfaces, as analog computing platforms to implement ANNs [21,25–29]. The wave-based dynamics of artificially engineered structures can be constructed as a mathematical isomorphism of digital ANNs so that structural parameters can be optimized by using the training framework of ANNs according to task objectives. Intelligent analog information processing tasks are directly performed in the native domain as physical waves propagate through the structures. Therefore, the speed of information processing is just the speed of wave propagation, and at the same time, no ADC and additional power consumption are introduced. Recently, optical and acoustic diffractive neural networks have been implemented by

---

*qbhe@sjtu.edu.cn

using metasurfaces for image recognition with ultrafast computation speed and low energy cost [26–28]. In these studies, the spatial scattering properties of waves between metasurface layers mimic the working principle of feed-forward neural networks with spatial hierarchy. This type of neural network structure is suitable for processing spatial wave fields, but not for processing time-series signals that are very common in human activity and mechanical vibrations.

Recurrent neural networks (RNNs) are particularly suitable for processing temporal signals due to their memory capabilities. The output of RNNs not only depends on the current input, but also on the state at the previous time step. Researchers have revealed that the dynamics of wave-based physical phenomena can be mapped into the computation in a digital RNN [25,30]. In the optimized structures, waves interact with each other in both spatial and temporal domains. The past state can be memorized in the dynamical behaviors of structures, making this neural network architecture inherently suitable for processing time series. However, for low-frequency vibrations propagating in solid media, wavelengths are generally very large compared to the device size. Current analog RNN design principles based on the scattering mechanism [25] and coupled mode theory [30] face intractable problems in low-frequency vibration identification because these methods cannot provide enough localized modes at low frequency. Besides, the connection between the intrinsic properties of the physical model and the frequency characteristics of signals has not been revealed. There are still knowledge gaps in terms of the design principles for identifying low-frequency vibrations (e.g., human activity and machinery vibration) end to end at the physical layer.

In this work, we propose a concept of a metamaterial-based analog RNN (Meta-RNN) with a simulated locally resonant elastic metamaterial. The proposed Meta-RNN is composed of local resonators coupled with each other. We establish a dynamical model of the metamaterial and analogize its computation process of dynamical response to a digital RNN. Owing to the coupling and synergy of local resonators, the metamaterial can achieve sufficiently complex vibration modes and frequency extraction capabilities to distinguish the patterns contained in excitation signals. By introducing the training framework of RNN, the vibration energy of the metamaterial can be learned to be localized at specific regions according to the task objectives. The Meta-RNN is verified to be able to perform accurate classification of Gaussian-modulated signals and practical machinery vibration signals. The proposed Meta-RNN provides a foundation for implementing a mechanical analog machine learning processor, providing inspiration for efficient information processing platforms towards machine intelligence.

II. CONCEPT OF META-RNN

The concept of the Meta-RNN implemented using an elastic metamaterial is illustrated in Fig. 1(a). The elastic metamaterial without damping is composed of local resonators with matrix mass M, resonator mass m, and resonator stiffness k_n. These local resonators are coupled by springs k_c. A vibration excitation is applied on the matrix of a local resonator on one side. The vibration responses of the optimized metamaterial are picked up by the measuring probes, which are the resonators of the corresponding unit cells. By comparing the normalized output energy obtained from the probes, the label of the highest energy output can be defined as the class of the input signal. As a proposal of physical implementation, we can use energy harvesters with a rectifier circuit to light LEDs to represent the class of excitation signals. In this way, the entire analog Meta-RNN can be implemented without any external power input.

The dynamical equation of the elastic metamaterial without damping can be expressed as

$$\mathbf{M\ddot{u}} + \mathbf{Ku} = \mathbf{f},\tag{1}$$

where $\mathbf{M}$ is a mass matrix with M and m, $\mathbf{K}$ is a stiffness matrix with k_c and k_n, reflecting the coupling relationship of the local resonators, $\mathbf{u}$ contains the displacement field of the metamaterial, and $\mathbf{f}$ is the external excitation applied on the metamaterial (see Appendix A for derivation with damping). The time-discretized dynamical equation with a temporal step of Δt can be expressed through the centered finite differences as

$$\frac{\mathbf{u}_{t+1} - 2\mathbf{u}_t + \mathbf{u}_{t-1}}{\Delta t^2} + \mathbf{M}^{-1}\mathbf{K}\mathbf{u}_t = \mathbf{M}^{-1}\mathbf{f}_t,\tag{2}$$

where the subscript t denotes the vector at a given time step. We express this dynamical equation as the matrix form

$$\begin{bmatrix} \mathbf{u}_{t+1} \\ \mathbf{u}_t \end{bmatrix} = \begin{bmatrix} \mathbf{2} - \Delta t^2 \mathbf{M}^{-1}\mathbf{K} & -\mathbf{1} \\ \mathbf{1} & \mathbf{0} \end{bmatrix} \begin{bmatrix} \mathbf{u}_t \\ \mathbf{u}_{t-1} \end{bmatrix} + \begin{bmatrix} \Delta t^2 \mathbf{M}^{-1} \\ \mathbf{0} \end{bmatrix} \mathbf{f}_t.\tag{3}$$

The convergence of the solution is associated with the time step. To evaluate the convergence of the solution, we set the time step (i.e., the sampling frequency of the discrete time series) to unit one. The dynamical equation can be written as

$$\begin{bmatrix} \mathbf{u}_{t+1} \\ \mathbf{u}_t \end{bmatrix} = \begin{bmatrix} \mathbf{2} - \mathbf{M}^{-1}\tilde{\mathbf{K}} & -\mathbf{1} \\ \mathbf{1} & \mathbf{0} \end{bmatrix} \begin{bmatrix} \mathbf{u}_t \\ \mathbf{u}_{t-1} \end{bmatrix} + \begin{bmatrix} \mathbf{M}^{-1} \\ \mathbf{0} \end{bmatrix} \tilde{\mathbf{f}}_t.\tag{4}$$
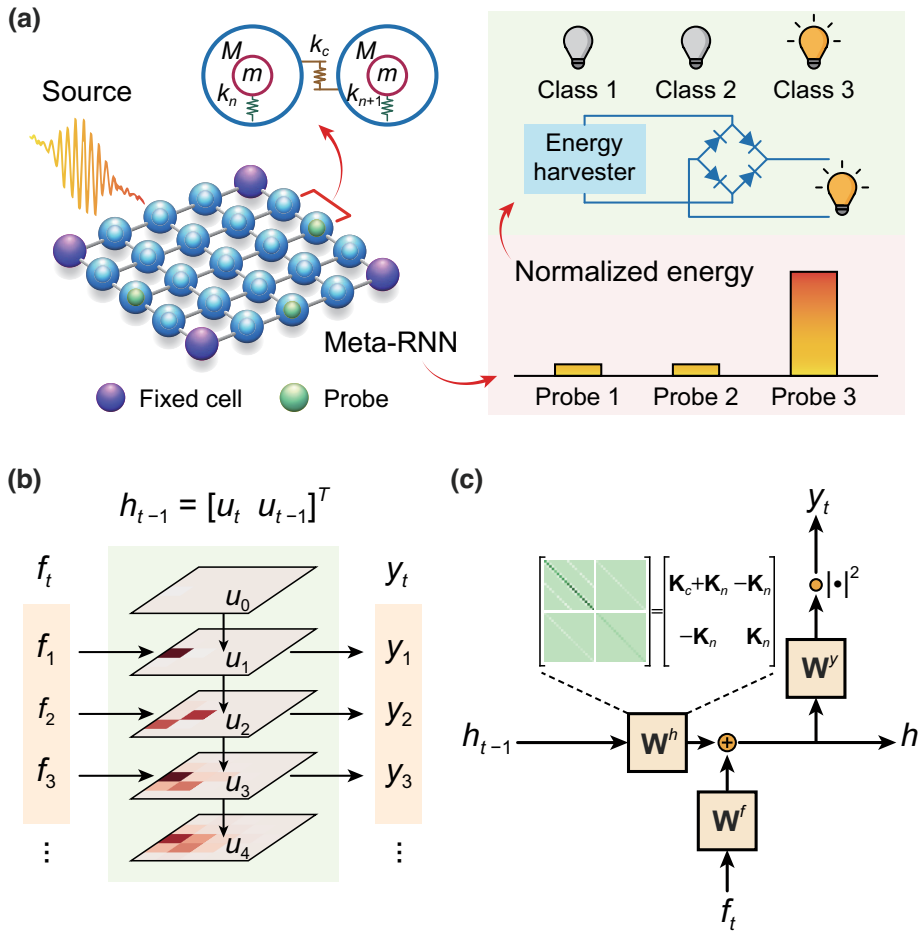
FIG. 1. Concept of the Meta-RNN. (a) Schematic diagram of the Meta-RNN. The column graph illustrates the output energy of the measuring probes as the predicted probability distribution for vibration information classification. (b) The recurrence relation of the Meta-RNN. The displacement fields at different time steps memorize the internal states of the metamaterial. (c) The internal component of the Meta-RNN cell, and the update process of the hidden state.

Once the maximum natural frequency $f_n^{\max}$ of the coupled dynamical model with the normalized $\tilde{\mathbf{K}}$ satisfies $\pi f_n^{\max} < 1$, the solution to Eq. (4) converges for arbitrary discrete time excitation. The real stiffness parameters can be obtained by $\mathbf{K} = f_s^2 \tilde{\mathbf{K}}$, where f_s is the sampling frequency of the excitation signal. Then, we define the hidden state of the metamaterial by using the displacement field at the current and preceding time steps as $\mathbf{h}_{t-1} = [\mathbf{u}_t, \mathbf{u}_{t-1}]^T$. Here, T is the notation of matrix transpose. The dynamical equation can thus be written in a recurrence form

$$\mathbf{h}_t = \mathbf{W}^h \mathbf{h}_{t-1} + \mathbf{W}^f \tilde{\mathbf{f}}_t, \qquad (5)$$

where $\mathbf{W}^h$ and $\mathbf{W}^f$ denote the corresponding matrices in Eq. (4) respectively. The output response $\mathbf{y}_t$ and time-integrated energy $\mathbf{E}_t$ of the metamaterial can be expressed by

$$\mathbf{y}_t = |\mathbf{W}^y \mathbf{h}_t|^2, \qquad (6)$$

$$\mathbf{E}_t = \sum_t \mathbf{y}_t, \qquad (7)$$

where $\mathbf{W}^y$ is the operator to extract the displacements of the measuring probes. The recurrence relation reveals

that the metamaterial system is capable of memorizing the internal hidden state in the displacement field [Fig. 1(b)]. The updating of the hidden state is determined by the intrinsic property of the metamaterial and the external excitation [Fig. 1(c)]. The output of the metamaterial at a given time not only depends on the input signal $\mathbf{f}_t$ at that time, but also on the state of the device $\mathbf{h}_{t-1}$ at the previous time step. As time evolves, the vibration energy can be concentrated at specific regions due to the learned vibration energy localization, thereby enabling the metamaterial to identify the mechanical vibrations. This process is similar to a digital RNN with the common form (see Appendix A). Different from the digital RNN, the weight $\mathbf{W}^h$ of the Meta-RNN is sparse, mainly determined by stiffness matrices $\mathbf{K}_c$ and $\mathbf{K}_n$ [Fig. 1(c)]. The stiffness matrix $\mathbf{K}_c$ contains the trainable parameters k_c, reflecting the coupling relationship of the local resonators. The stiffness matrix $\mathbf{K}_n$ includes the trainable stiffness of local resonators k_n. To quantify the predicted probability distribution of the Meta-RNN's output, we calculate the time-integrated energy $\mathbf{E}_t$ at each probe. After the Meta-RNN evolves for the duration of the excitation signal, we integrate the final values of $\mathbf{E}_t$ into a vector, and normalize the vector by using the sum of the values. This normalized vector $\mathbf{E}_{\text{norm}}$ can be

defined as the predicted probability distribution over the signal classes. We calculate the cross-entropy loss function between the predicted probability distribution and the label. To train the system, we use backpropagation to compute the gradients of the cross-entropy loss function with respect to the trainable parameters, and perform gradient descent to reduce the loss. By using the ADAM optimization algorithm to update the trainable structural parameters of the metamaterial k_c and k_n, the patterns of excitation signals can thus be recognized (see Appendix B for details of the computation process of Meta-RNN).

III. RESULTS

A. Verification on synthetic signals

We first use a simulated dataset to investigate the performance of the proposed Meta-RNN. The simulated dataset consists of the Gaussian-modulated pulse signals with a signal-to-noise ratio (SNR) of 0 dB (see Fig. S1 of the Supplemental Material [31]). The signals are divided into three classes according to the center frequencies of 30, 50, and 70 Hz with the sampling frequency of 1 kHz. Each

signal class contains 1000 samples. We use 80% of the samples for training and the remaining 20% for testing. To ensure that the loss can eventually converge, the learning rate is set to decay exponentially during the training process. After 20 training epochs, the cross-entropy loss value drops from 1.21 to 0.59 [see Fig. S2(a) of the Supplemental Material [31]]. After training, we conduct the testing process and calculate the cross-entropy loss value as 0.59. The optimized metamaterial can recognize the excitation signals with an accuracy ratio of 100% [see Figs. S2(b) and S2(c) of the Supplemental Material [31] for the confused matrix of the classification results and parameter distributions of k_n and k_c]. To analyze the dynamical response of the metamaterial, we respectively select a sample from each signal class to excite the metamaterial, and extract the vibration responses at the measuring probes [Fig. 2(a)]. The response amplitude of the probe corresponding to the true label is significantly larger than that of the other two probes. The predicted probability distributions are also consistent with the true labels [Fig. 2(b)].

To understand the working mechanism of the Meta-RNN, we calculate the responses of the trained
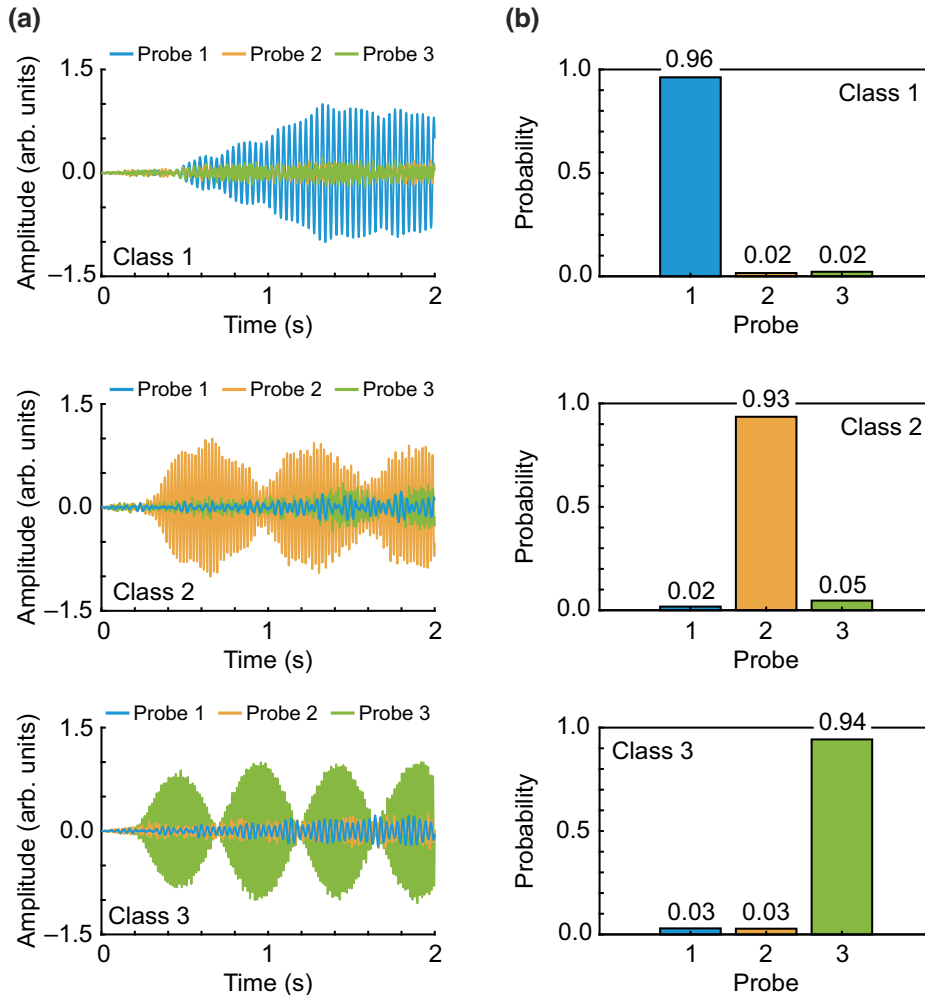

FIG. 2. Classification performance of the Meta-RNN for the Gaussian-modulated pulse signals. (a) The vibration responses at the measuring probes when the metamaterial is excited by the signals with different center frequencies. (b) The predicted probability distributions of the Meta-RNN for three classes of signals.
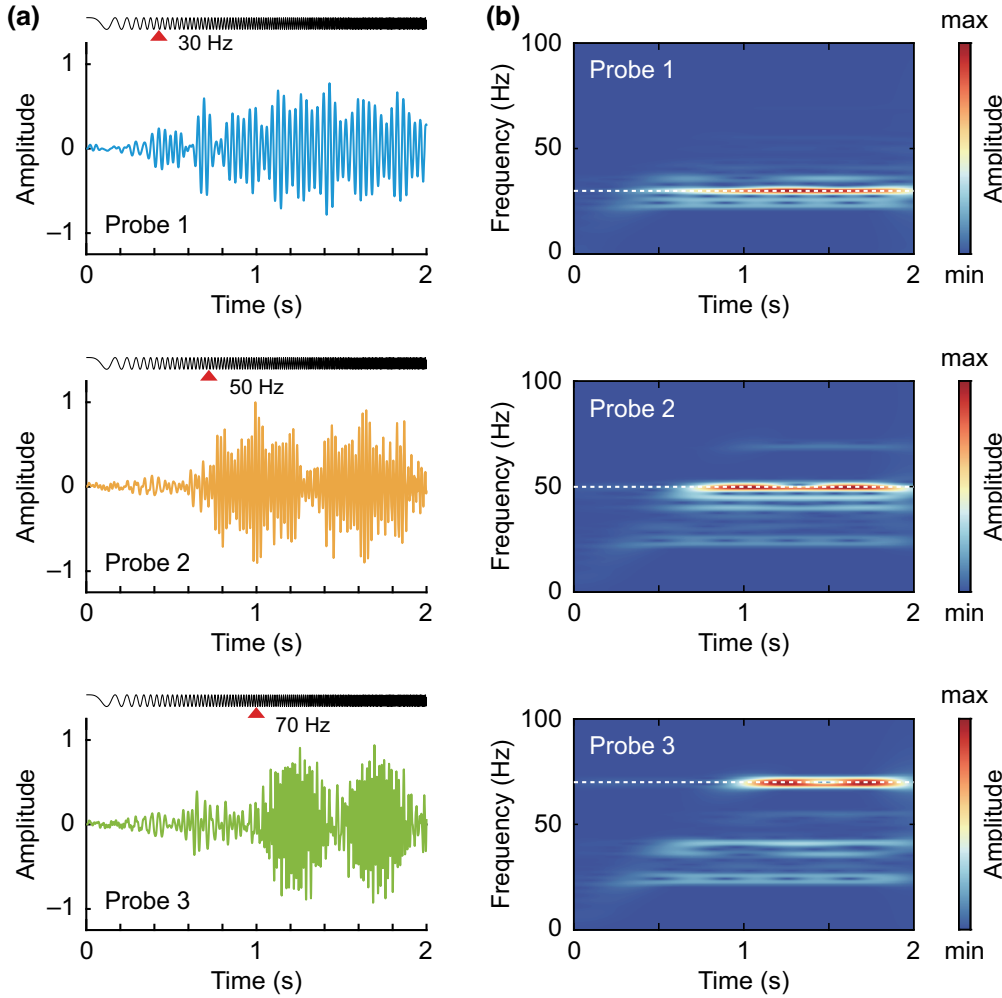
FIG. 3. Vibration responses of the metamaterial. (a) Temporal responses under the excitation of linear frequency-modulated signals. The red triangles denote the corresponding instants of the frequencies. (b) Time-frequency spectra of the responses obtained at three measuring probes. The white dashed lines denote the frequencies of 30, 50, and 70 Hz.

metamaterial excited by a linear frequency-modulated signal. From the responses obtained at the measuring probes, it can be seen that the metamaterial starts to amplify the signals when excitation evolves to the time positions corresponding to the center frequencies of the Gaussian-modulated pulse signals [Fig. 3(a)]. The spectrograms of the responses at different probes show that the metamaterial is sensitive to the characteristic frequencies, presenting a frequency selectivity [Fig. 3(b)]. This phenomenon indicates that the Meta-RNN is capable of learning intrinsic patterns of the excitation signals. Similar frequency sensitivity (i.e., frequency filtering characteristics) has also been observed in biological neural systems [32–34].

To further verify the working mechanism of the Meta-RNN, we define a metric called the relative frequency transfer function to compare the vibration amplification effect of the three measuring probes as

$$T = 20 \log_{10} \frac{T_i^2}{T_j T_k}, \tag{8}$$

where the variables T with subscripts i, j, and k denote the responses of three measuring probes. The calculated metric

T shows that the metamaterial can amplify some characteristic frequency components (29.8, 48.8, and 70.3 Hz) at one measuring probe and suppress the components at the other two probes (Fig. 4). This phenomenon indicates that the metamaterial can discover the intrinsic patterns contained in the mechanical vibrations.

We respectively calculate the vibration displacement fields of the resonators excited at the three characteristic frequencies [Fig. 5(a)]. Benefiting from the well-trained coupled local resonators, the vibration energy can be localized at the corresponding probes. This means that specific regions of the metamaterial can be selectively activated according to the input information. This learned energy localization mechanism has some similarities to the local activation of brains in response to external stimuli [35]. To evaluate the contribution of each order of vibration mode to the response, we define the normalized modal participation factor Q_r as

$$Q_r = |q_r| / \sum_r |q_r|,$$

$$q_r = \mathrm{rms} \left(\frac{\mathbf{v}_r^{\mathrm{T}} \mathbf{M} \mathbf{u}}{\mathbf{v}_r^{\mathrm{T}} \mathbf{M} \mathbf{v}_r} \right), \tag{9}$$
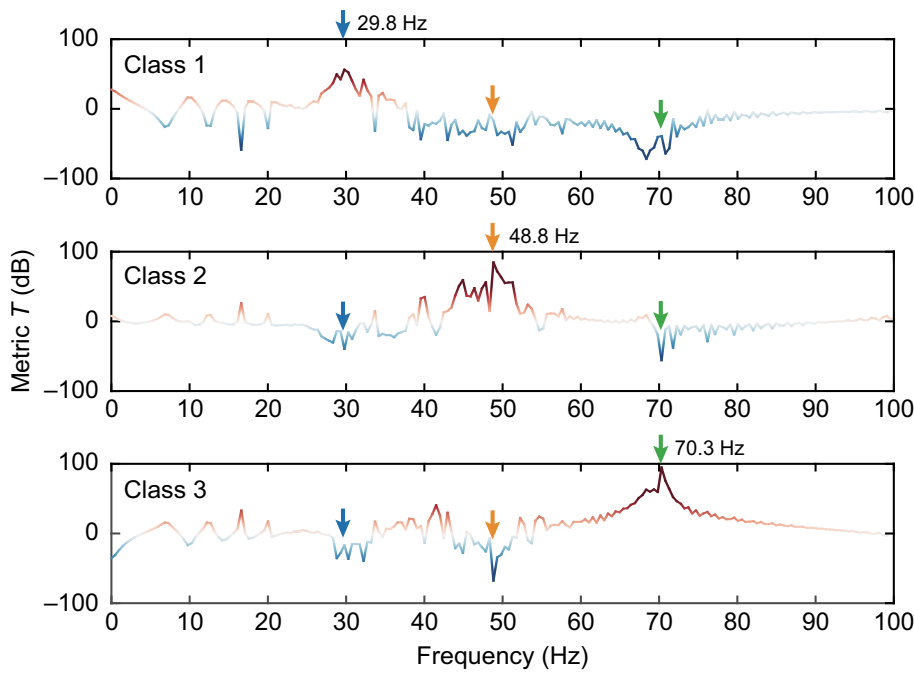
FIG. 4. The metric T calculated from three measuring probes of the metamaterial optimized based on the Gaussian pulse dataset.

where $\mathbf{v}_r$ is the rth order modal vector, and rms($\cdot$) is the root-mean-square operator for the time series. It can be noticed that a certain order of vibration mode provides most of the contribution [Fig. 5(b)], and the modal frequencies are very close to the local resonance frequencies of the unit cells at the measuring probes (32.9, 54.6, and 71.1 Hz). Therefore, for signals with simple frequency components, such as Gaussian pulses, the local resonance of unit cells can provide sufficient learning ability for the Meta-RNN.
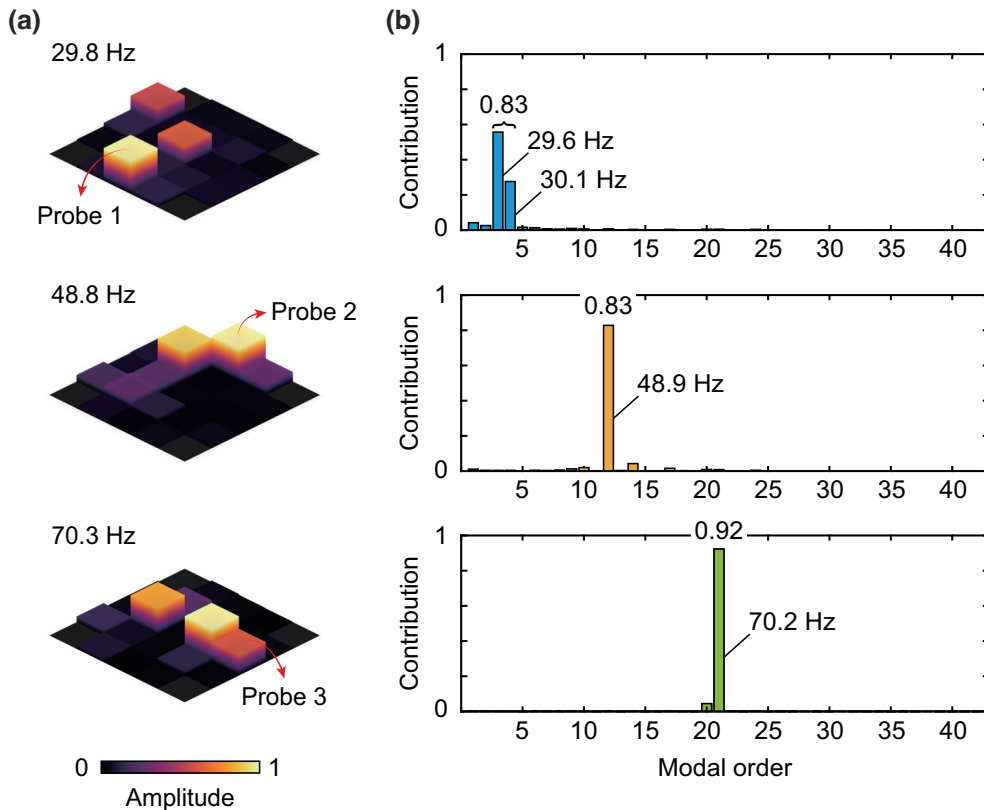

FIG. 5. Modal analysis of the trained metamaterial based on Gaussian pulses. (a) Vibration displacement fields of the resonators at the excitation frequencies of 29.8, 48.8, and 70.3 Hz. (b) Modal contribution of the vibration modes at the corresponding excitation frequencies.
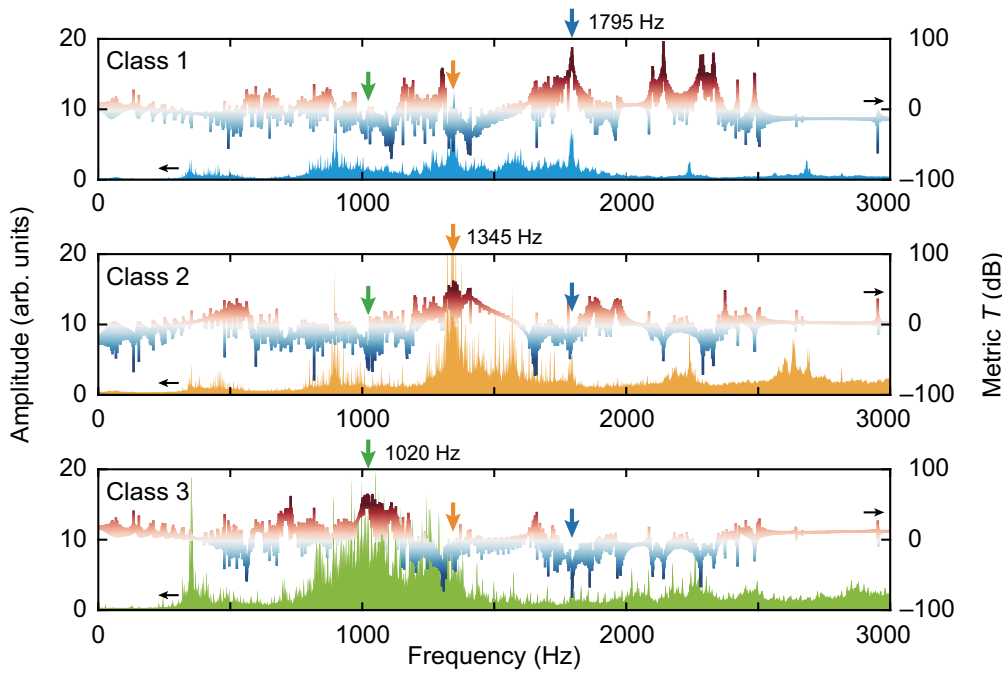
FIG. 6. The metric T calculated from the trained metamaterial and the mean frequency spectra of the machine vibration signals.

B. Verification on practical signals

To demonstrate the universality of the proposed Meta-RNN, we collect a dataset including three types of vibration signals from an industrial machine as the input of the metamaterial for vibration information classification (see Fig. S3 of the Supplemental Material [31]). The vibration signals with the sampling frequency of 10 240 Hz reflect three machine health states including normal condition, slight fault, and severe fault. We retrain the Meta-RNN with 3000 samples and test the classification performance with 270 samples. After 40 training epochs, the accuracy ratio of classification is 100%, indicating that the
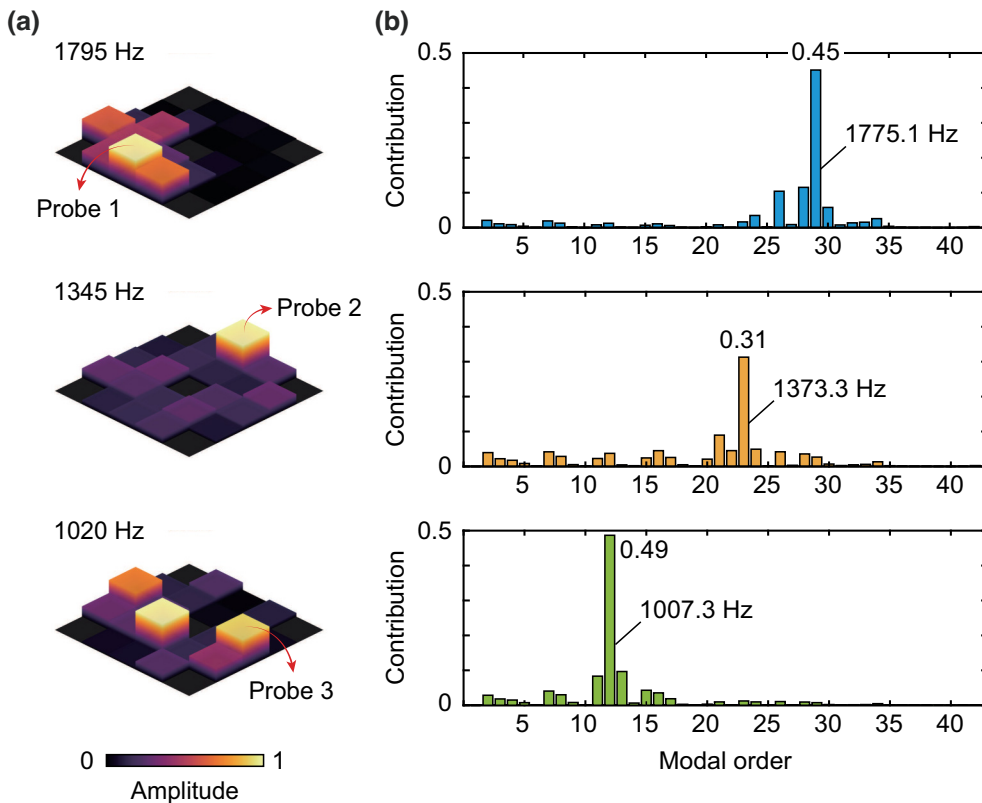

FIG. 7. Modal analysis of the metamaterial optimized based on the practical machine vibration signals. (a) Vibration displacement distributions at the frequencies marked by arrows in Fig. 6. (b) Modal contribution of the vibration modes at the corresponding excitation frequencies.
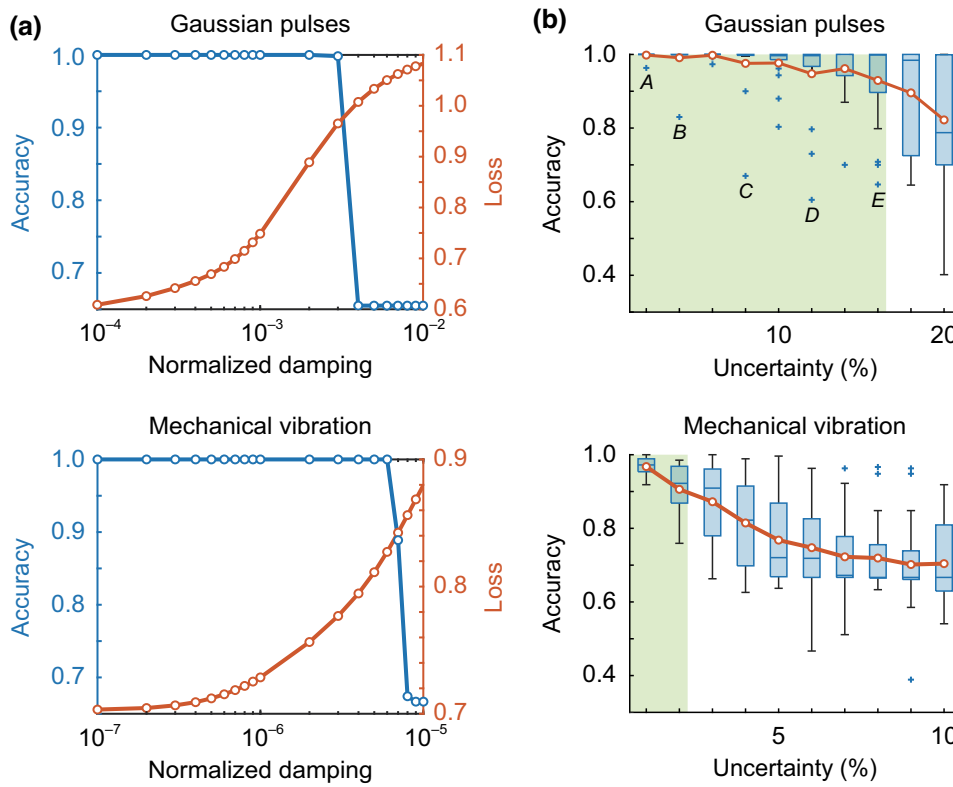
FIG. 8. Factors effecting the performance of the Meta-RNN. (a) The relationships between the damping and the recognition accuracy for two types of datasets. (b) The relationships between the uncertainty and the recognition accuracy. The orange solid lines denote the average classification accuracy. The blue plus signs denote the outliers.

Meta-RNN can still discover useful knowledge in such complex vibration signals (see Fig. S4 of the Supplemental Material [31] for the optimized stiffness parameter distribution and the confused matrix). The responses of the Meta-RNN and the predicted probability distributions are obtained from the measuring probes (see Fig. S5 of the Supplemental Material [31]), which are consistent with the true labels.

We also calculate the metric T to verify the frequency extraction properties of the Meta-RNN on the practical machine signals. The comparison between the metric T and the frequency spectra of machine signals shows that the metamaterial can also learn the patterns of machine signals by amplifying the characteristic frequency bands at the measuring probes (Fig. 6). The vibration displacement distributions at the frequencies of 1795, 1345, and 1020 Hz [Fig. 7(a)] show that the vibration energy can be localized at the measuring probes after learning. Different from the results in Fig. 5(b), the vibration energy localization is contributed to by multiple vibration modes [Fig. 7(b)], which means that the learning ability of the Meta-RNN mainly depends on the coupling and synergy of the local resonators for signals with complex components. The metamaterial with capabilities of condition monitoring and identification is hoped to be integrated with industrial machines for ultrafast information processing without power consumption, thereby empowering machines with intelligence.

C. Parameter analysis

To analyze the effects of damping on the performance of the Meta-RNN, we conduct calculations based on these two datasets by adding damping c_n and c_c to the optimized Meta-RNN trained without damping. From the relationships between the damping and recognition accuracy [Fig. 8(a)], we can conclude that the performance of the Meta-RNN is robust when the building materials have smaller energy loss (e.g., metals). We also investigate the effects caused by the uncertainty of the trainable parameters on the recognition accuracy of the Meta-RNN [Fig. 8(b)]. The parameter variations in 20 calculations follow an unbiased Gaussian distribution with the uncertainty as the variance. The tolerable parameter uncertainty (where the average classification accuracy is larger than 90%) is 16% for the Gaussian pulses and 2% for the practical machinery vibration signals, which indicates that more complex signal classification requires higher structural parameter accuracy. More analysis about the outliers *A–E* in Fig. 8(b) and the parameter uncertainties with different distributions can be found in Appendix C. This uncertainty analysis provides guidance to control the manufacturing tolerance for the physical realization of the Meta-RNN.

IV. DISCUSSION

We propose a strategy for metamaterial-based analog RNNs to perform vibration signal classification in their

native domain. Since the metamaterial-based platform does not involve ADC and data storage, information processing can be realized with ultrafast processing speed and no power consumption. The proposed dynamical model of the metamaterial is simple but still significant because any continuous structure can be discretized and converted to the equation with the form of mass-spring-damping matrices. Although the proposed Meta-RNN is a theoretical model, this study takes the first step towards mechanical metamaterial-based machine intelligence. Compared with the works that train physical systems to produce desired responses [36], we build a metamaterial model that is mathematically isomorphic to the digital RNN for intelligent low-frequency vibration information processing. The metamaterial can be trained under the learning framework of the RNN, which is applicable for identifying various types of vibration signals end to end. The Meta-RNN can be considered as a neural system of mechanical systems, thereby enabling the possibility of intelligent machines.

Our study has some advantages over previous works in terms of design principles. The proposed model is based on the coupled network with local resonators, which is particularly suitable for dealing with low-frequency vibrations. The complexity of coupling ensures that efficient identification performance can be achieved using a small number of unit cells. In Ref. [25], the analog computation is essentially based on the diffraction of waves. The inverse-designed medium with inhomogeneous wave speed is realized by the binary distribution of material mass density. This means that a large device size (approximately 10λ in width) is needed to route the wave energy to the desired positions, which is not suitable for processing low-frequency vibrations. Although Ref. [30] can use resonance to design a single unit cell on a subwavelength scale, the coupling in the waveguides is simple, leading to bulky device size (60 resonators in each waveguide and about 62λ in length) to deal with low-frequency vibrations. Besides, we reveal the connection between the intrinsic properties of the trained metamaterial model and signal characteristics. The coupling stiffness and local resonators are optimized to achieve selective frequency extraction and energy localization at specific unit cells. Therefore, we can use a small number of coupled local resonators to discover useful knowledge in low-frequency vibrations.

There are also some important issues that should be discussed in the following aspects for improvement. In the real physical model, vibrations are very complex because they contain multiple modes such as bending and torsional modes. Therefore, we should consider more vibration modes in the dynamical modeling of the metamaterial. The moment of inertia and spring masses also need to be considered in dynamic modeling. For identification tasks with more signal classes, the number of local resonators needs to be increased to provide more internal states and local vibration modes. At present, the training process does not

involve the real physical system because the Meta-RNN has not been physically realized. In fact, the gap between the simulated model and the real physical model, including the manufacturing tolerances and the bias in parameter updates during training, is another important issue that affects the physical implementation of the Meta-RNN. These challenging problems should be addressed before building an effective physical model of the Meta-RNN. Fortunately, some proposed schemes may provide avenues to address these issues. In Ref. [20], a universal framework is demonstrated to train real physical systems as deep neural networks by performing backpropagation through a digital model of the physical system and sending the trained input parameters to the physical system. In addition to backpropagation method, a physics-driven learning system implemented by circuitry is proposed based on a contrastive learning scheme to allow self-adjusting of the network [37]. Although these approaches involve additional digital circuits and external electrical power inputs, which is inconsistent with the goal of achieving a fully analog Meta-RNN, they can still provide inspiration for the future physical implementation of the Meta-RNN. Furthermore, the energy conversion efficiency at the output of the physical model is also an important factor affecting classification performance. In this work, the characteristic frequency components of signals can be amplified by coupled local resonators, so that the output power can be enhanced to ensure the classification performance of the system. In the future, materials with high sensitivity and high electromechanical conversion efficiency (e.g., flexible piezoelectric films and triboelectric materials) can be used to generate more power to improve the sensing bound.

In conclusion, we demonstrate a concept of an analog RNN with trained locally resonant metamaterials for low-frequency vibration information classification in its native domain. The learned low-frequency vibration energy localization enables the metamaterial to extract intrinsic features contained in mechanical vibrations. We provide the basic theory that guides the physical implementation of the Meta-RNN. Our proposed approach presents a promising mechanical analog processor of machine learning, with the potential to perform computation more efficiently than its digital counterparts. This study can not only open attractive avenues to endow machines with intelligence, but also provide inspiration in designing intelligent devices for wearable vital sign recognition (e.g., body movement, cardiopulmonary function, and muscle degeneration) and earthquake detection, thereby offering rich opportunities to novel sensing paradigms for health monitoring, human-machine interaction, and the Internet of things.

APPENDIX A: DYNAMICS OF METAMATERIAL WITH DAMPING

For the elastic metamaterial with damping, the dynamical equation can be expressed as

$$\mathbf{M}\ddot{\mathbf{u}} + \mathbf{C}\dot{\mathbf{u}} + \mathbf{K}\mathbf{u} = \mathbf{f}. \tag{A1}$$

The time-discretized equation is given by using the centered finite differences as

$$\frac{\mathbf{u}_{t+1} - 2\mathbf{u}_t + \mathbf{u}_{t-1}}{\Delta t^2}$$

$$+ \mathbf{M}^{-1}\mathbf{C}\frac{\mathbf{u}_{t+1} - \mathbf{u}_{t-1}}{2\Delta t} + \mathbf{M}^{-1}\mathbf{K}\mathbf{u}_t = \mathbf{M}^{-1}\mathbf{f}_t. \tag{A2}$$

The recurrent relationship can thus be derived as

$$\begin{bmatrix} \mathbf{u}_{t+1} \\ \mathbf{u}_t \end{bmatrix} = \begin{bmatrix} (1+\boldsymbol{\Omega})^{-1}(2 - \Delta t^2\mathbf{M}^{-1}\mathbf{K}) & (1+\boldsymbol{\Omega})^{-1}(-1+\boldsymbol{\Omega}) \\ 1 & 0 \end{bmatrix} \begin{bmatrix} \mathbf{u}_t \\ \mathbf{u}_{t-1} \end{bmatrix} + \begin{bmatrix} \Delta t^2(1+\boldsymbol{\Omega})^{-1}\mathbf{M}^{-1} \\ 0 \end{bmatrix} \mathbf{f}_t,$$

$$\boldsymbol{\Omega} = \frac{1}{2}\Delta t\mathbf{M}^{-1}\mathbf{C}. \tag{A3}$$

The dynamical equation is very similar to the form of the common digital RNN, which can be expressed as

$$\mathbf{h}_t = \sigma^h(\mathbf{W}^h\mathbf{h}_{t-1} + \mathbf{W}^x\mathbf{x}_t), \tag{A4}$$

$$\mathbf{y}_t = \sigma^y(\mathbf{W}^y\mathbf{h}_t), \tag{A5}$$

where $\mathbf{h}_t$ is the hidden state; $\mathbf{x}_t$ and $\mathbf{y}_t$ are the input and output of the digital RNN, respectively; $\mathbf{W}^h$, $\mathbf{W}^x$, and $\mathbf{W}^y$ are weight matrices; and $\sigma^h(\cdot)$ and $\sigma^y(\cdot)$ are activation functions. Different from the Meta-RNN, the weight matrix $\mathbf{W}^h$ here is a dense matrix.

APPENDIX B: DETAILS OF THE COMPUTATION PROCESS OF THE META-RNN

The proposed Meta-RNN is simulated using the open source platform PYTORCH. The training and testing process are conducted on a remote host with Intel(R) Xeon(R) CPU Platinum 8260L at 2.30 GHz and 80 GB of RAM. In the training process, the gradient of the cross-entropy loss function with respect to the trainable parameters is automatically calculated in PYTORCH. We use the ADAM algorithm to optimize the parameters. The batch size is set to ten. The learning rate decays exponentially with the rate of 0.992 in each batch. To avoid the parameters being negative, we use a function $f(x) = \max(0, x)$ to handle the updated parameters.

For the Gaussian-modulated pulse signals, the sampling frequency is 1 kHz. The signals can be expressed as

$$s(t) = \left(1 - \cos\frac{2\pi f_0}{11}t\right)\sin(2\pi f_0 t) + n(t), \tag{B1}$$

where f_0 is the center frequency of the pulse, and $n(t)$ is the additive white Gaussian noise with the SNR of 0 dB. The waveforms and spectra of the three types of signal samples can be found in Fig. S1 of the Supplemental Material [31]. In the training process on this dataset, m and M are set as 35.26×10^{-3} and 13.03×10^{-3} kg, respectively. The normalized trainable parameters k_n are initialized with uniformly distributed random numbers from 1.0×10^{-3} to 7.0×10^{-3}. The normalized trainable parameters k_c are initialized with 5.0×10^{-3}. The initial learning rate is set as 1×10^{-4}.

The industrial machinery vibration signals are acquired with the sampling frequency of 10 240 Hz from a planetary gear box including three planetary gears. The rotation speed of the motor is 1600 rev/min. The gear modulus is 1.5. The teeth number of the ring gear, planetary gears, and sun gear are 84, 31, and 21, respectively. The first class of signals reflects the normal state of the gearbox. The second class of signals reflects the slight failure of the gear box with a broken tooth in the ring gear. The third class of signal reflects the severe fault of the gear box, in which both the ring gear and the sun gear have a broken tooth. The waveforms and spectra of three types of signal samples can be found in Fig. S3 of the Supplemental Material [31]. In the training process on this dataset, m and M are set as 0.5×10^{-3} and 2×10^{-3} kg, respectively. The normalized trainable parameters k_n are initialized with uniformly distributed random numbers from 0 to 1.0×10^{-3}. The normalized trainable parameters k_c are initialized with uniformly distributed random numbers from 0.2×10^{-3} to 1.0×10^{-3}, respectively. The initial learning rate is set as 2×10^{-5}.

APPENDIX C: FURTHER ANALYSIS OF THE PARAMETER UNCERTAINTY

We analyze the outliers *A–E* [Fig. 8(b)] with low recognition accuracy for Gaussian pulses by calculating the metric *T* of each Meta-RNN model [see Fig. S6(a) of the Supplemental Material [31]]. Compared to the cases with the same parameter uncertainty and high recognition accuracy [see Fig. S6(b) of the Supplemental Material [31]], the parameter uncertainties of the outliers affect the extraction ability of the characteristic frequencies. We further analyze the parameter uncertainties with different distributions (see Fig. S7 of the Supplemental Material [31]). The parameters are multiplied by coefficients μ_{k_c} and μ_{k_n} on the basis of the original values to simulate systematic errors, and the uncertainties still follow a Gaussian distribution. For Gaussian pulses, the Meta-RNN model shows robustness within a 10% uncertainty. However, for machine vibration signals, biased parameter distributions have significant influences on the performance of the model. The results also indicate that the coupling and synergy of local resonators are the key to the learning ability of the Meta-RNN from another perspective.

---

[1] Y. Jiang, Z. Liu, N. Matsuhisa, D. Qi, W. R. Leow, H. Yang, J. Yu, G. Chen, Y. Liu, C. Wan, Z. Liu, and X. Chen, Auxetic mechanical metamaterials to enhance sensitivity of stretchable strain sensors, Adv. Mater. **30,** e1706589 (2018).

[2] F. Yi, Z. Zhang, Z. Kang, Q. Liao, and Y. Zhang, Recent advances in triboelectric nanogenerator-based health monitoring, Adv. Funct. Mater. **29,** 1808849 (2019).

[3] T. Jiang, C. Li, Q. He, and Z. K. Peng, Randomized resonant metamaterials for single-sensor identification of elastic vibrations, Nat. Commun. **11,** 2353 (2020).

[4] T. Jiang, X. Liao, H. Huang, Z.-K. Peng, and Q. He, Scattering-coded architectured boundary for computational sensing of elastic waves, Cell Rep. Phys. Sci. **3,** 100918 (2022).

[5] F. Wen, Z. Zhang, T. He, and C. Lee, AI enabled sign language recognition and VR space bidirectional communication using triboelectric smart glove, Nat. Commun. **12,** 5378 (2021).

[6] Z. Hu, Y. Zhang, and S. Pan, in *Proceedings of the 19th ACM Conference on Embedded Networked Sensor Systems*, Coimbra, Portugal, (2021).

[7] H. Cui, R. Hensleigh, D. Yao, D. Maurya, P. Kumar, M. G. Kang, S. Priya, and X. R. Zheng, Three-dimensional printing of piezoelectric materials with designed anisotropy and directional response, Nat. Mater. **18,** 234 (2019).

[8] D. Maurya, S. Khaleghian, R. Sriramdas, P. Kumar, R. A. Kishore, M. G. Kang, V. Kumar, H. C. Song, S. Y. Lee, Y. Yan, J. M. Park, S. Taheri, and S. Priya, 3D printed graphene-based self-powered strain sensors for smart tires in autonomous vehicles, Nat. Commun. **11,** 5392 (2020).

[9] Q. Han, Z. Ding, Z. Qin, T. Wang, X. Xu, and F. Chu, A triboelectric rolling ball bearing with self-powering and self-sensing capabilities, Nano Energy **67,** 104277 (2020).

[10] W. Xiong, C. Zhu, D. Guo, C. Hou, Z. Yang, Z. Xu, L. Qiu, H. Yang, K. Li, and Y. Huang, Bio-inspired, intelligent flexible sensing skin for multifunctional flying perception, Nano Energy **90,** 106550 (2021).

[11] Y. LeCun, Y. Bengio, and G. Hinton, Deep learning, Nature **521,** 436 (2015).

[12] G. Hinton, L. Deng, D. Yu, G. Dahl, A.-R. Mohamed, N. Jaitly, A. Senior, V. Vanhoucke, P. Nguyen, T. Sainath, and B. Kingsbury, Deep neural networks for acoustic modeling in speech recognition: The shared views of four research groups, IEEE Signal Process Mag. **29,** 82 (2012).

[13] C. D. M. Julia Hirschberg, Advances in natural language processing, Science **349,** 261 (2015).

[14] B. Sanchez-Lengeling and A. Aspuru-Guzik, Inverse molecular design using machine learning: Generative models for matter engineering, Science **361,** 360 (2018).

[15] J. Jumper, R. Evans, A. Pritzel, T. Green, M. Figurnov, O. Ronneberger, K. Tunyasuvunakool, R. Bates, A. Žídek, and A. Potapenko, Highly accurate protein structure prediction with AlphaFold, Nature **596,** 583 (2021).

[16] W. Ma, F. Cheng, and Y. Liu, Deep-learning-enabled on-demand design of chiral metamaterials, ACS Nano **12,** 6326 (2018).

[17] G. X. Gu, C.-T. Chen, D. J. Richmond, and M. J. Buehler, Bioinspired hierarchical composite design using machine learning: simulation, additive manufacturing, and experiment, Mater. Horiz. **5,** 939 (2018).

[18] C. Qian, B. Zheng, Y. Shen, L. Jing, E. Li, L. Shen, and H. Chen, Deep-learning-enabled self-adaptive microwave cloak without human intervention, Nat. Photonics **14,** 383 (2020).

[19] F. Zangeneh-Nejad, D. L. Sounas, A. Alù, and R. Fleury, Analogue computing with metamaterials, Nat. Rev. Mater. **6,** 207 (2020).

[20] L. G. Wright, T. Onodera, M. M. Stein, T. Wang, D. T. Schachter, Z. Hu, and P. L. McMahon, Deep physical neural networks trained with backpropagation, Nature **601,** 549 (2022).

[21] M. S. S. Rahman, J. Li, D. Mengu, Y. Rivenson, and A. Ozcan, Ensemble learning of diffractive optical networks, Light Sci. Appl. **10,** 14 (2021).

[22] C. Du, F. Cai, M. A. Zidan, W. Ma, S. H. Lee, and W. D. Lu, Reservoir computing using dynamic memristors for temporal information processing, Nat. Commun. **8,** 2204 (2017).

[23] S. Kumar, J. P. Strachan, and R. S. Williams, Chaotic dynamics in nanoscale NbO$_2$ Mott memristors for analogue computing, Nature **548,** 318 (2017).

[24] C. Wang, S. J. Liang, C. Y. Wang, Z. Z. Yang, Y. Ge, C. Pan, X. Shen, W. Wei, Y. Zhao, Z. Zhang, B. Cheng, C. Zhang, and F. Miao, Scalable massively parallel computing using continuous-time data representation in nanoscale crossbar array, Nat. Nanotechnol. **16,** 1079 (2021).

[25] T. W. Hughes, I. A. D. Williamson, M. Minkov, and S. Fan, Wave physics as an analog recurrent neural network, Sci. Adv. **5,** eaay6946 (2019).

[26] X. Lin, Y. Rivenson, N. T. Yardimci, M. Veli, Y. Luo, M. Jarrahi, and A. Ozcan, All-optical machine learning using diffractive deep neural networks, Science **361,** 1004 (2018).

[27] J. Li, D. Mengu, N. T. Yardimci, Y. Luo, X. Li, M. Veli, Y. Rivenson, M. Jarrahi, and A. Ozcan, Spectrally encoded single-pixel machine vision using diffractive networks, Sci. Adv. **7,** eabd7690 (2021).

[28] J. Weng, Y. Ding, C. Hu, X. F. Zhu, B. Liang, J. Yang, and J. Cheng, Meta-neural-network for real-time and passive deep-learning-based object recognition, Nat. Commun. **11,** 6309 (2020).

[29] A. Momeni and R. Fleury, Electromagnetic wave-based extreme deep learning with nonlinear time-Floquet entanglement, Nat. Commun. **13,** 2651 (2022).

[30] Y. Qu, M. Zhou, E. Khoram, N. Yu, and Z. Yu, Resonance for analog recurrent neural network, ACS Photonics **9,** 1647 (2022).

[31] See Supplemental Material at http://link.aps.org/supplemental/10.1103/PhysRevApplied.19.064065 for the figures of input signals and more computational results of the Meta-RNN.

[32] B. Hutcheon and Y. Yarom, Resonance, oscillation and the intrinsic frequency preferences of neurons, Trends Neurosci. **23,** 216 (2020).

[33] S. Stagkourakis, C. T. Perez, A. Hellysaz, R. Ammari, and C. Broberger, Network oscillation rules imposed by species-specific electrical coupling, eLife **7,** e33144 (2018).

[34] J. Vera, U. Pereira, B. Reynaert, J. Bacigalupo, and M. Sanhueza, Modulation of frequency preference in heterogeneous populations of theta-resonant neurons, Neuroscience **426,** 13 (2020).

[35] T. H. Kim, G. W. Jeong, H. S. Baek, G. W. Kim, T. Sundaram, H. K. Kang, S. W. Lee, H. J. Kim, and J. K. Song, Human brain activation in response to visual stimulation with rural and urban scenery pictures: A functional magnetic resonance imaging study, Sci. Total Environ. **408,** 2600 (2010).

[36] C. P. Goodrich, A. J. Liu, and S. R. Nagel, The Principle of Independent Bond-Level Response: Tuning by Pruning to Exploit Disorder for Global Behavior, Phys. Rev. Lett. **114,** 225501 (2015).

[37] S. Dillavou, M. Stern, A. J. Liu, and D. J. Durian, Demonstration of Decentralized Physics-Driven Learning, Phys. Rev. Appl. **18,** 014040 (2022).